ACS APPLIED MATERIALS & INTERFACES

Research Article

www.acsami.org

Understanding Side Reactions in K–O_2 Batteries for Improved Cycle Life

Xiaodi Ren,[†] Kah Chun Lau,[‡,§] Mingzhe Yu,[†] Xuanxuan Bi,[†] Eric Kreidler,[⊥] Larry A. Curtiss,[‡,§] and Yiying Wu*[,†]

[†]Department of Chemistry and Biochemistry, The Ohio State University, 100 West 18th Avenue, Columbus, Ohio 43210, United States

[‡]Materials Science Division and [§]Joint Center for Energy Storage Research, Argonne National Laboratory, Argonne, Illinois 60439, United States

[⊥]Honda Research Institute USA, Inc., 1381 Kinnear Road, Columbus, Ohio 43212, United States

Supporting Information

ABSTRACT: Superoxide based metal–air (or metal–oxygen) batteries, including potassium and sodium–oxygen batteries, have emerged as promising alternative chemistries in the metal–air battery family because of much improved round-trip efficiencies (>90%). In order to improve the cycle life of these batteries, it is crucial to understand and control the side reactions between the electrodes and the electrolyte. For potassium–oxygen batteries using ether-based electrolytes, the side reactions on the potassium anode have been identified as the main cause of battery failure. The composition of the side products formed on the anode, including some reaction intermediates, have been identified and quantified. Combined experimental studies and density functional theory (DFT) calculations show the side reactions are likely driven by the interaction of potassium with ether molecules and the crossover of oxygen from the cathode. To inhibit these side reactions, the incorporation of a polymeric potassium ion selective membrane (Nafion-K^+) as a battery separator is demonstrated that significantly improves the battery cycle life. The K–O_2 battery with the Nafion-K^+ separator can be discharged and charged for more than 40 cycles without increases in charging overpotential.

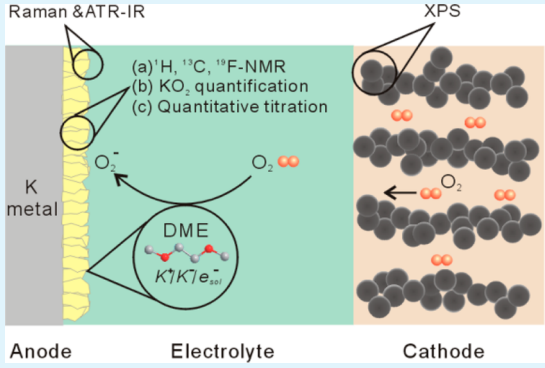

KEYWORDS: *metal–air batteries, potassium–oxygen battery, side reactions, O_2 crossover, ion selective separator*

INTRODUCTION

In recent years, metal–air batteries, especially nonaqueous lithium–air batteries (or Li–O_2 batteries), have drawn considerable worldwide research attention for future energy storage applications because of the high theoretical energy density (3505 Wh/kg).[1−5] However, Li–O_2 batteries, with the formation of the insulating Li_2O_2 as the discharge product, are plagued by electrolyte and the carbon cathode instability in addition to a low round-trip power efficiency (<60%) resulting from high charging potentials (>4.0 V vs Li^+/Li).[6−8] In contrast, superoxide based batteries, namely potassium–oxygen (K–O_2) and sodium–oxygen (Na–O_2) batteries developed by our group and the Adelhelm group, display much improved round-trip efficiencies (greater than 90%) in the absence of any electrocatalysts.[9,10] Instead of forming peroxide species during discharge, K–O_2 and Na–O_2 batteries stabilize the superoxide intermediate to generate potassium superoxide (KO_2) and sodium superoxide (NaO_2). The improved electronic conductivity of KO_2 reported in previous literature[11] should help to eliminate the problem of charge transport as observed in Li–O_2 batteries.[12,13] More importantly, the quasi-reversible one-electron redox reaction ($O_2 + e^- \leftrightarrow O_2^-$) is characterized by fast charge-transfer kinetics and low overpotentials[9,14,15] which are particularly beneficial during the charging process. Despite of lower specific energy densities compared to Li–O_2 batteries, metal–air batteries based on superoxide products provide promising solutions for energy storage applications where efficiency and cost are more significant than weight concerns, as in smart grid and renewable energy storage applications.

Although the concept of superoxide based batteries with high round-trip efficiencies has been demonstrated, continuous overpotential increases were observed and the batteries displayed limited cycle lives.[9,15,16] In our study, the insulating surface layer formed on the potassium anode of K–O_2 batteries employing ethers as the solvent was suspected to be the primary reason for battery failure since the replacement of the anode restored the initial small discharge/charge potential gap[9] and extended battery life. The surface layer on the K anode, which is analogous to the solid-electrolyte interface (SEI) layer in lithium-ion batteries (LIB), assumes the role of metal cation

Received: August 9, 2014
Accepted: October 8, 2014
Published: October 8, 2014

conduction.[17] Although the formation of a thin SEI layer on graphite in LIBs has proven to be important for stabilizing the anode, the apparent overgrowth of the surface layer on K anodes due to side reactions may result in suppressed ion transport. This increases the battery internal resistance and ultimately leads to battery failure. The side reactions can also deplete the electrolyte and the metal anode, inhibiting long-term battery operation.

In spite of the urgency to overcome the problems induced by the anode surface layer to increase battery cycle life, a detailed understanding of the formation mechanism of the surface layer is obscured by the complicated nature of the system. The highly reductive potassium metal is known to have reactions with ether molecules which results in electrolyte decomposition.[18,19] Additionally, the crossover of O_2 molecules to the anode could have a substantial impact. In recent studies of Li−O_2 batteries with ether electrolytes, similar phenomena have been reported. Shui et al. used in situ X-ray diffraction to reveal a continuous accumulation of LiOH on Li metal anodes during both discharge and charge processes.[20] Assary et al. have studied the influence of oxygen crossover on the Li anode which showed the existence of carbonate and carbonyl species along with LiOH.[21] The mechanism of decomposition of ether molecules on the Li anode was proposed on the basis of DFT calculations; however, insight into the surface layer growth is greatly limited by the lack of a detailed compositional analysis.

Here, a detailed analysis of the components for the anode surface layer in K−O_2 batteries is provided with supporting theoretical DFT calculations to verify the proposed decomposition reaction pathways. Considering the shared high reducing characteristics of alkali metals, it is hoped that this study would also provide insight on the anode behavior in Li−O_2 and Na−O_2 batteries. Moreover, in order to restrict the crossover of species between the anode and the cathode, a polymeric ion-selective membrane (Nafion-K^+) was incorporated into the cell design and was found to largely improve the battery cycle life.

EXPERIMENTAL SECTION

Preparation of Nafion-K^+ membrane. Ion selective membranes were prepared using a previously reported method with modifications.[22] To exchange the original cation (H^+) of Nafion to K^+, Nafion 211 membranes (25 μm thickness, DuPont) were heated in a 0.5 M KOH solution of dimethyl sulfoxide (DMSO) (>99.9%, Sigma-Aldrich) and water (volume ratio=1:1) at 60 °C for 2 h. The residual solvent and KOH were removed by stirring the membrane in distilled water at 90 °C for 2 h. The Nafion-K^+ membranes were dried under vacuum at 100 °C overnight and then soaked for ∼12 h in the battery electrolyte before use.

Cell assembly and tests. Swagelok cells were constructed by stacking a potassium anode (99.5%, Sigma-Aldrich), two glass fiber separators (300 μm thickness, GF/A, Whatman) with a piece of as-prepared Nafion-K^+ membrane sandwiched in-between, and a porous cathode under high purity Argon. For surface layer composition analysis on the potassium, P50 carbon paper (14 mm diameter, AvCard) was used as the cathode and the Nafion-K^+ membrane was omitted from the cell construction. The electrolyte used was 0.5 M KPF_6 (99.5%, Sigma-Aldrich) in 1,2-dimethoxyethane (DME) (Novolyte). The battery was sealed by Viton O-rings except at the gas inlet. Solvents and oxygen gas (99.993%, UHP) are further dried by molecular sieves (3A, Sigma-Aldrich) before use in the battery tests. The batteries were conditioned with O_2 gas at 1 atm pressure for 2 h before testing. Galvanostatic discharge/charge tests were carried out using a Maccor test station (Model 4304) or a MTI battery analyzer (BST8-MA) with the lower and upper cutoff voltages set at 2.0 and 3.0 V (vs K^+/K), respectively. The current density used was 65 μA/cm^2 (geometric area).

For battery cycle life tests, an oxygen electrode with Super P carbon powder (kindly provided by Timcal) on a Ni foam framework was used. Carbon loadings were approximately 10 mg and the electrodes were fabricated using a preparation method previously described.[9] No PTFE binder was included to avoid possible interference with XPS characterization. The discharge capacities were set to 0.6 mAh and the charging processes were cutoff at 3.0 V (vs K^+/K).

Characterization methods. Characterization of the anode surface layer composition was performed after removing the surface layers following either full battery discharge to 2.0 V or after 4 discharge/charge cycles to 0.6 mAh discharge capacity. Raman and attenuated total reflectance infrared (ATR-IR) spectroscopies were initially employed to characterize the main components in the surface layer. The Raman spectra were collected on a Raman spectrometer (inVia, Renishaw) with an excitation wavelength of 633 nm (laser power 6 mW) using an airtight sample holder with a quartz optical window. The infrared data were obtained by using an ATR-IR spectrometer equipped with a diamond window (PerkinElmer, Frontier) inside a glovebox. The ratio of KOH to K_2CO_3 was determined by comparing the area ratios of the absorption peaks at 3500 cm^{-1} (from KOH) and 1400 cm^{-1} (from K_2CO_3) versus a calibration curve. The calibration curve was generated from measurements of KOH (99.99%, Sigma-Aldrich) and K_2CO_3 (99.99%, Sigma-Aldrich) powder mixtures with different molar ratios.

The surface layer samples were then dissolved in D_2O (99.9%, Sigma-Aldrich) for ^{1}H, ^{13}C and ^{19}F nuclear magnetic resonance (NMR) measurements on a 400 MHz NMR spectrometer (Bruker, Avance III). To quantify the organic side products in the surface layer, a known amount of DMSO was added as an internal reference. As no apparent fluoride decomposition species were found from the ^{19}F-NMR spectra, a known amount of KF (>99.99%, Sigma-Aldrich) was added to quantify the content of residual KPF_6 in the surface layer. D_2O was also used to extract species remaining in the battery cathode after cycling for ^{1}H NMR tests following similar procedures.

The amount of potassium superoxide was determined by a method reported in previous literature.[15] Portions of surface layer samples were first reacted with water, and the concentration of H_2O_2 generated was quantified based on the UV−vis absorbance (Lambda 950 Spectrometer, PerkinElmer) after adding diluted Titanium(IV) oxysulfate ($TiO(SO_4)$) solution (∼2%, Sigma-Aldrich). According to the reaction eqs 1 and 2, the amount of KO_2 was calculated.

$$2KO_2 + 2H_2O \rightarrow 2KOH + H_2O_2 + O_2 \quad (1)$$

$$TiO(SO_4) + H_2O_2 \rightarrow [Ti(O_2)]^{2+}SO_4^{2-} + H_2O \quad (2)$$

The D_2O solutions of the surface layer samples used for NMR tests were then titrated using 0.01 N HCl solution (Sigma-Aldrich). The titration curves were plotted by monitoring the change of pH values with a pH meter (Acron ion 6, Oakton) vs HCl amount. The total amount of HCl

consumed was used to quantify the respective amounts of KOH and K_2CO_3 in the surface layer given the stoichiometric relationships of the following reactions.

$$KOH + HCl \rightarrow KCl + H_2O \quad (3)$$

$$K_2CO_3 + 2HCl \rightarrow 2KCl + H_2O + CO_2 \quad (4)$$

$$R - COOK + HCl \rightarrow R - COOH + KCl \quad (5)$$

(R: CH_3, H or $CH_3O - CH_2$)

Note, the amount of KO_2, HCOOK, CH_3COOK, and CH_3OCH_2COOK as well as the ratio of KOH to K_2CO_3 are known from previous measurements.

Analysis of the gas phase reaction products between potassium and DME were carried out using the headspace gas chromatography−mass spectrometry (GC-MS) method on a Thermo Scientific DSQ-II GC-MS system. The electrolyte solution (0.5 M KPF_6 in DME) was prepared by bubbling Ar gas to remove residual dissolved O_2 before mixing with small pieces of potassium metal and molecular sieves. The mixtures were stored in septum-sealed vials for 1 week prior to analysis. Molecular sieves were utilized to prevent scavenging of potassides and solvated electrons by any H_2O generated during the reaction process. A gastight syringe (Pressure-lok glass syringe, Vici) was used for headspace sampling and 5 μL of the gaseous samples were injected directly into the GC column (Restek Rtx-5MS), which separated the gaseous reaction products from the DME vapor for MS analysis (electron impact ionization (EI) mode, 70 eV).

X-ray photoelectron spectroscopy (XPS) analysis of the carbon powder in the cathode after the battery cycle life testing was performed to probe possible changes to the carbon surface. The carbon powders inside the Ni foam framework were dispersed in DME by sonication. The suspension was then drop-cast onto a clean Si wafer inside a glovebox and the DME was allowed to evaporate before analysis. The sample was transferred from the glovebox to the XPS chamber using an airtight transfer module. The spectra were collected on a Kratos Axis Ultra XPS spectrometer using monochromatic Al Kα radiation. An electron flood gun was used for the test to avoid possible surface charging problems. All spectra were calibrated by referencing the C 1s peak position of the C−C peak at a binding energy of 284.8 eV. Spectra curve fitting was performed using a combined Gaussian−Lorentzian profile after a Shirley-type background subtraction using the CasaXPS program.

Computational methods. Density functional theory (DFT) was used to model the electrochemical stability of DME on the anode side in the presence of O_2. The 6-31G +(d,p) basis set was used and the zero point vibration energy, enthalpy, and Gibbs free energy (at 298.15 K, 1 atm) were calculated at the level of B3LYP/6-31+G(d,p) using Gaussian09 code.[23]The Polarizable Continuum Model (PCM) at the B3LYP/6-31+G(d,p) (or B3LYP/6-31+G**) level was used to calculate the free energies of solvation for the reaction species at the optimized geometries. To mimic a DME environment in solution phase, a dielectric constant (ε) of 7.2 was used in all PCM calculations. The transition state of the reaction was first located and then judged by the intrinsic reaction coordinate (IRC) algorithm as implemented in the Gaussian09 code. The reduction potential (E^0) of the electrolyte (i.e., DME solvent) relative to K^+/K reference electrode was determined by using

$E^0 = (\Delta G^{solution}_{(298K)}/nF) - 1.53$ V, where $\Delta G^{solution}_{(298K)}$ is the free energy change during the reduction process, n is the number of electron transferred, and F is Faraday's constant.

RESULTS AND DISCUSSION

Side Reactions at the Potassium Metal Electrode. During initial battery testing, replacing the potassium anode was found to provide additional capacity as shown in Figure 1.

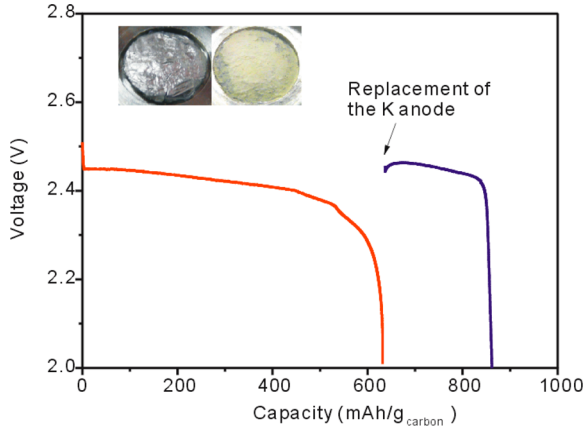

Figure 1. Voltage−capacity curve for a K−O_2 battery discharged to 2.0 V. (Blue line indicates the resumed discharge process with the replacement of the K anode. The inset pictures show the change of the anode after test.)

The initial discharge with a P50 carbon paper cathode delivered a capacity of 630 mAh/g_{carbon}. After discharge, a yellow surface layer was observed on the anode surface (see inset of Figure 1). After the potassium anode was replaced, an additional capacity of 230 mAh/g_{carbon} was obtained. This infers that the growth of the anode surface layer was the main reason for the potential decay observed at the end of the original discharge step. Similar behaviors were observed for battery cycle tests: although larger discharge/charge voltage gaps were observed with increasing cycles, small voltage gaps (charge/discharge overpotentials) could be restored after the potassium anode was replaced. To obtain insight into the potassium surface layer formation mechanism, the yellow layer covering the potassium anode was isolated for further analysis.

Raman and ATR-IR were employed to characterize the main components of the potassium surface layer. The anode surface layer sample obtained after cycling displayed a strong Raman signal from KO_2 (1143 cm^{-1}) along with vibrations from KOH, K_2CO_3 and KPF_6 (Figure 2a). ATR-IR (Figure 2b) also proved that aside from KO_2, the main species in the surface layer are KOH, K_2CO_3 and KPF_6. Similarly, LiOH and Li_2CO_3 were shown to be the main decomposition products on the anode in the Li−O_2 battery case.[21] The depletion of solvent as a result of decomposition and evaporation could precipitate out KPF_6 and thus is the postulated source of this signal. The formation of KO_2 (yellow color crystals) is likely due to the crossover of O_2 molecules from the porous cathode and its subsequent reaction with potassium. The quantification of KOH and K_2CO_3 content in cycled samples was carried out following the procedure described previously. A similar surface layer of about 300 μm thick was observed on the potassium surface soaked in the electrolyte under O_2 atmosphere for 24 h (see Figure S1 in the Supporting Information). It is worth noting that exactly the same species in the sample obtained after potassium aging in

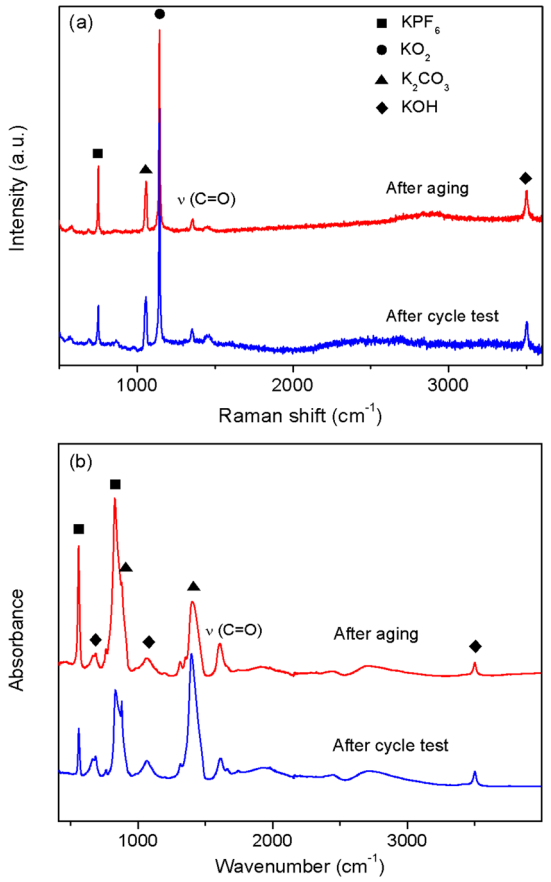

Figure 2. (a) Raman and (b) ATR-IR spectra of the metal surface layers formed after aging in electrolyte under O_2 atmosphere or battery cycle test.

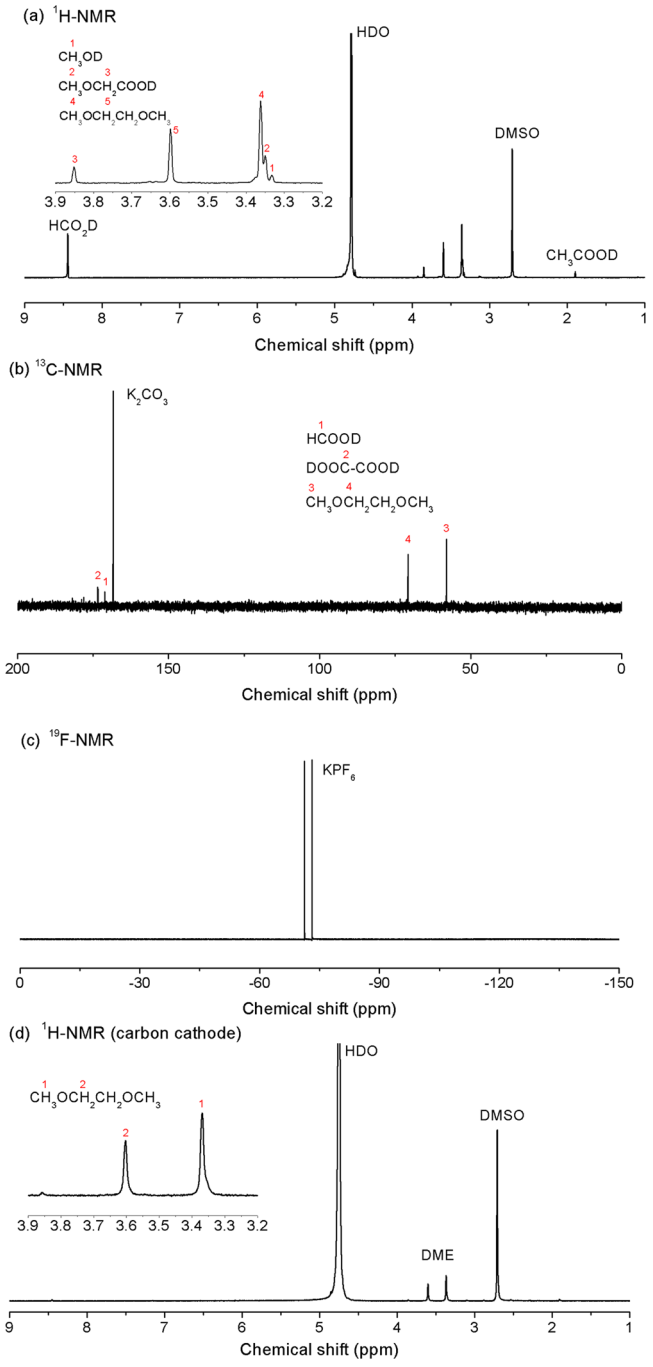

Figure 3. (a) ^{1}H NMR (with DMSO reference), (b) ^{13}C NMR, (c) ^{19}F-NMR spectra of the anode surface layer in D_2O solution after battery cycle tests; (d) ^{1}H NMR spectrum of extracts from the P50 carbon cathode in D_2O solution after battery cycle tests (with DMSO reference). All the species are written in the form after deuterium ion exchange.

the electrolyte solution were observed by Raman and IR as with the samples obtained after battery cycling. While a detailed quantification of the aged sample surface layer composition was not performed due to limitations of sample quantity, the relative Raman signal intensities of KO_2, KOH and K_2CO_3 in the aged sample were lower compared to the cycled sample. This result implies that the growth of the anode surface layer is a spontaneous process and is independent of charging or discharging the potassium anode. A more detailed discussion is provided in the following sections.

In addition to the inorganic species detected, the identities of organic side products were verified using NMR spectroscopy. As shown in Figure 3a, in the D_2O solution of the surface layer sample, potassium formate (HCOOK; δ = 8.44 ppm, singlet), potassium acetate (CH_3COOK; δ = 1.90 ppm, singlet), potassium methoxide (CH_3OK; δ = 3.34 ppm, singlet) and potassium methoxyacetate (CH_3OCH_2COOK; δ = 3.85 ppm, singlet, -OCH_2−COOK; δ = 3.35 ppm, singlet, CH_3O−) together with residual DME were identified. The ^{13}C NMR spectrum of the D_2O solutions (Figure 3b) also verified the existence of K_2CO_3 and a small amount of potassium formate. Furthermore, a signal mostly likely from potassium oxalate ($K_2C_2O_4$) was detected at δ = 173.4 ppm. Potential signals from other species may be too weak to be observed from ^{13}C NMR. The ^{19}F-NMR spectrum only showed a signal from KPF_6 and no apparent decomposition from KPF_6 was observed (Figure 3c). The use of DME as a model ether solvent and the NMR spectroscopy have made feasible the verification of all the structures of side products on the potassium anode. The identification of methoxyacetate and oxalate species has been proved valuable for decomposition mechanism modeling.

The proton-containing species contained in the surface layer were quantified by ^{1}H NMR using DMSO as an internal reference. A known amount of KF was added to the solution for the quantification of KPF_6 using ^{19}F-NMR. However, potassium oxalate was not quantified due to the limitations of ^{13}C NMR and Raman/IR, which may be a source of error for

the analysis. More details concerning the quantification procedures can be found in the Experimental Section. As shown in Table 1, the anode surface layers obtained from

Table 1. Components in the Anode Surface Layer after Battery Cycle or Discharge Tests (5 Individual Measurements)

	weight percentage (%)				
	after cycle tests			after discharge	
	A	B	C	D	E
KO_2	22.2	20.5	22.1	27.2	26.1
KPF_6	10.7	9.7	12.9	13.4	15.4
KOH	44.3	48.0	42.9	41.2	39.5
K_2CO_3	5.2	6.0	8.0	5.9	6.3
organic side products	2.6	2.7	3.9	4.3	5.0
sum	85.0	86.9	89.8	92.0	92.3

battery cycle tests contain approximately 30−35 wt % KO_2 and KPF_6, 45−55 wt % of the side products KOH and K_2CO_3, and less than 5 wt % of proton-containing decomposition intermediates. The results suggest that the decomposition of DME on the potassium anode is a favored process. Additionally, similar composition ratios were observed for batteries after single full discharge tests. Due to the shorter times for discharge vs cycling tests, KO_2 and KPF_6 comprise a larger weight percentage of the layer composition and the decomposition products (KOH and K_2CO_3) appear in relatively smaller ratios. An accelerated film growth during battery testing compared to the aging condition was observed and is likely due to the dynamic formation of new potassium/electrolyte interfaces during potassium electrodissolution and electrodeposition; however, there is no clear evidence that electrolyte decomposition is faster in either charge or discharge processes. The unspecified 7−15 wt % mass in the surface layers may be due to potassium oxalate, glass fibers from the separator, residual DME, and/or from quantification errors because of the limited sample amounts and methods employed. Also, it is worth mentioning that although it is believed that the basic growth mechanism of the surface layers are the same regardless of test conditions, the exact composition of the anode surface layer would be dependent on the specific test environment (O_2 pressure, current density, battery configurations) and may change when test parameters are varied.

Formation Mechanism of Side Products. As mentioned earlier, the battery anode environment is complicated by the presence of highly reducing potassium metal and crossover O_2 molecules. The influences of both factors need to be taken into account to interpret the anode side reaction mechanism. The interaction of potassium with ether molecules was proposed to be the side reaction initiator. Because of the chelating ability of oxygen atoms in ether molecules to alkali metal cations (especially potassium and sodium), metal dissolution are known to occur in several solvents (e.g., DME, tetraglyme and solvents with proper crown ethers[24,25]). The resulting solutions show characteristic blue colors as shown in Figure 4a for a DME solution and Figure S2 in the Supporting Information for 18-crown-6 in THF and tetraglyme. It is still unclear whether potassium anions (K^-, known as potasside) and/or solvated electrons are responsible for the blue color. It was suggested in previous studies that the blue color of potassium metal in ether solvents might be from potasside.[26] In

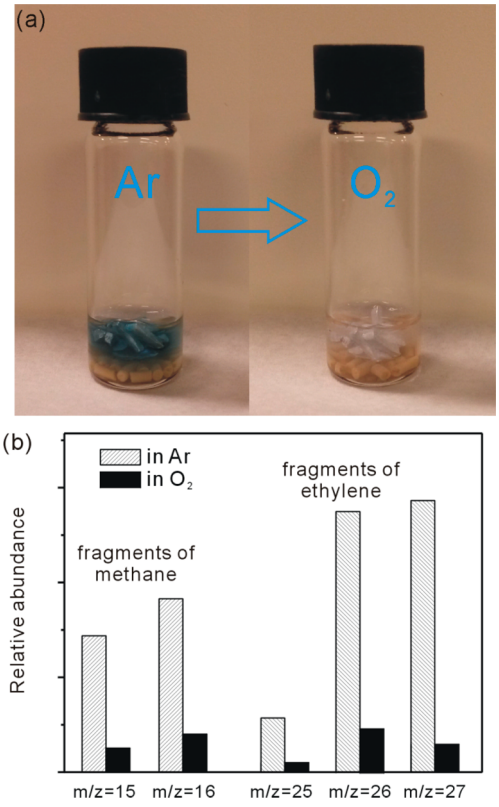

Figure 4. (a) Color change of the K metal solution in DME with 0.5 M KPF_6 before and after injection of dry oxygen gas. (b) GC-MS detection of selected gasous phase components after reaction between potassium and DME electrolyte under Ar or O_2 atmosphere (m/z = 15, 16 attributed to fragments of methane molecules; m/z = 25, 26, 27 to fragments of ethylene molecules; m/z = 28 signal not selected because possible N_2 contamination during sample injection).

our ^{39}K-NMR and EPR test of the potassium solution in tetrahydrofuran with 18-crown-6, signals of both potasside species (δ=-96.4 ppm)[27] and solvated electrons (g = 2.0017)[26] (Figures S3 and S4 in the Supporting Information) were detected along with the same blue color as in the potassium solution of DME. However, because of the low solubility of potassium in DME and tetraglyme as well as the unstable nature of the active species,[24] neither potasside nor solvated electron signals were detected in these two solvents. It is expected that the following equilibrium conditions exist in the potassium-ether system, as proposed in previous literature.[19]

$$M(s) + nL \leftrightarrow e^-, M^+L_n \quad (6)$$

$$M(s) + e^-, M^+L_n \leftrightarrow M^-, M^+L_n \quad (7)$$

where L = DME, tetraglyme, crown ethers, etc.

Depending on the structures of ether ligands, potassium cation concentration, and temperature etc., the shift of the equilibrium species will favor either potasside or solvated electron formation. In addition, it is quite possible that some ether solvent molecules could be reduced and exist in anionic form. Further study of the active species in alkali metal-ether systems is ongoing and will be reported later.

The direct reductive cleavage of C−O bonds in ethers by alkalids and/or solvated electrons has been reported in previous studies.[18,19] The detection of gas phase products (e.g., methane, and ethylene as shown in Figure 4b) and solution phase

Scheme 1. Proposed Mechanism of DME Decomposition on the Anode Side with Oxygen Crossover

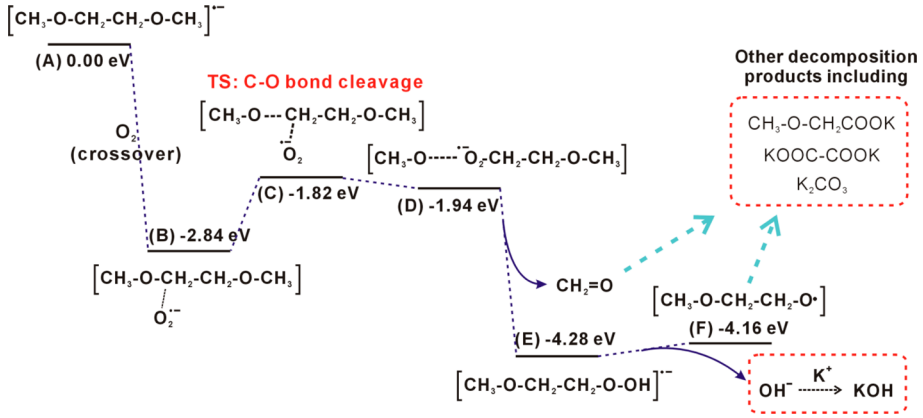

products (e.g., methoxide, 2-methoxy-ethoxide, ethoxide, etc., as shown in Figure S5 in the Supporting Information) after the reaction of potassium with DME confirms that DME decomposition can be induced through direct C−O bond cleavage by highly reductive species. However, as shown in Figure 4a, an immediate decay of the blue color in the potassium-DME solution was observed when dry oxygen gas was introduced into the system. This indicates a very fast electron transfer process from the potassides and solvated electrons to the O_2 molecules which would also occur in the working environment of K−O_2 batteries. Moreover, as shown in Figure 4b, the presence of O_2 significantly decreases the amounts of the characteristic gas side products (methane and acetylene) generated from direct reductive C−O cleavage reactions. This suggests that the observed side reactions on the anode side are not mainly induced by potassides and solvated electrons, but by the subsequent electron transfer to O_2 and the formation of superoxide (O_2^-) anion radicals which subsequently react. As discussed before, this process is spontaneous and would lead to the generation of KO_2 on the anode surface under an O_2 atmosphere (Figure 2a). On the basis of this understanding, the decomposition reactions on the anode will be accelerated in both discharge and charge processes through the exposure of fresh metal surfaces (K electrodissolution on discharge and electrodeposition on charge). The rapid accumulation of the side products on the anode would significantly hinder battery cycle life.

To probe the possible mechanism of DME decomposition on the K anode in the presence of crossover O_2 from the cathode (especially the formation of KOH and K_2CO_3), we used DFT calculations to assess the reductive stability of DME as shown in Scheme 1. From the DFT calculations, the computed reduction potential of DME in solution phase (ε = 7.2) is 1.26 eV relative to K, which suggests DME molecules may be reduced on the potassium anode through interaction with potasside or solvated electron species. O_2 in the vicinity of the anode is predicted to interact with the negatively charged DME radical (A) to form complex (B) through a very exothermic process quantified by an energy reduction of ∼2.8 eV. The oxygen-DME complex (B) results in the subsequent energetically favorable reaction pathways as shown in Scheme 1. In contrast to O_2^- anion radical attack on a neutral DME molecule in solution, which is likely to be much slower kinetically,[28,29] there is no apparent barrier for the subsequent C−O bond cleavage resulting from the DME-oxygen complex derived from the reaction path A → B. For negatively charged DME radicals (A), the extra electrons are localized at the methylene carbon (−CH_2−) sites thus making it a favorable binding site for any incoming species with high electron affinity. O_2 binds to the DME radical and is reduced to superoxide initiating C−O bond cleavage. Transition state (C) during C−O bond breaking is also found to be thermodynamically favorable with an energy reduction of 1.82 eV relative to O_2 and the DME radical. With this reaction pathway, the formations of KOH and K_2CO_3 are both found to be thermodynamically favorable through the formation of subsequent decomposition complexes (D, E and F) which are of lower energy than the initial reactant (A). From the intermediate dissociated complex (F), the presence of hydroxide (OH^-) can subsequently lead to the accumulation of insoluble and insulating KOH at the potassium anode surface if O_2 crossover continues to proceed. The experimentally observed K_2CO_3, potassium alkyl carbonates, and potassium acetate are found to be secondary parasitic reaction products after KOH (Table 1). The formation mechanism of these species may proceed due to the presence of decomposed fragments (e.g., alkoxy radicals and aldehydes) resulting from further electron transfer reactions with superoxide ions, hydrogen abstractions, and reaction with incoming solvated K^+ and O_2, as shown in Scheme S1 in the Supporting Information. It is proposed that the crossover of O_2 to the anode plays a significant role in promoting the decomposition of the DME electrolyte and the formation of the anode surface layer.

Effect of Nafion-K^+ Membrane on Battery Performance. As discussed above, oxygen crossover from the cathode induces increased side product formation on the anode and thus limits battery cycle life. The restriction of O_2 crossover to the anode (and DME anion radicals to the cathode) is expected to improve K−O_2 battery cyclability. To test this hypothesis, a polymeric K^+ ion-selective membrane (Nafion-K^+) was placed between the two glass fiber separators during cell construction. As shown in Figure 5, a marked increase in cycle life was observed between a battery with and without a Nafion-K^+ membrane separator. Without the K^+ ion selective separator, the discharge/charge potential gap increased significantly during the eighth and ninth cycles. In contrast, the Nafion-K^+ separator largely improved the battery cycle life, although the discharge/charge overpotential gap was increased to ∼0.3 V due to the resistance of the membrane. However, the potential gap was generally constant for more than 40 cycles. Moreover, Coulombic efficiencies were increased to greater than 98% for

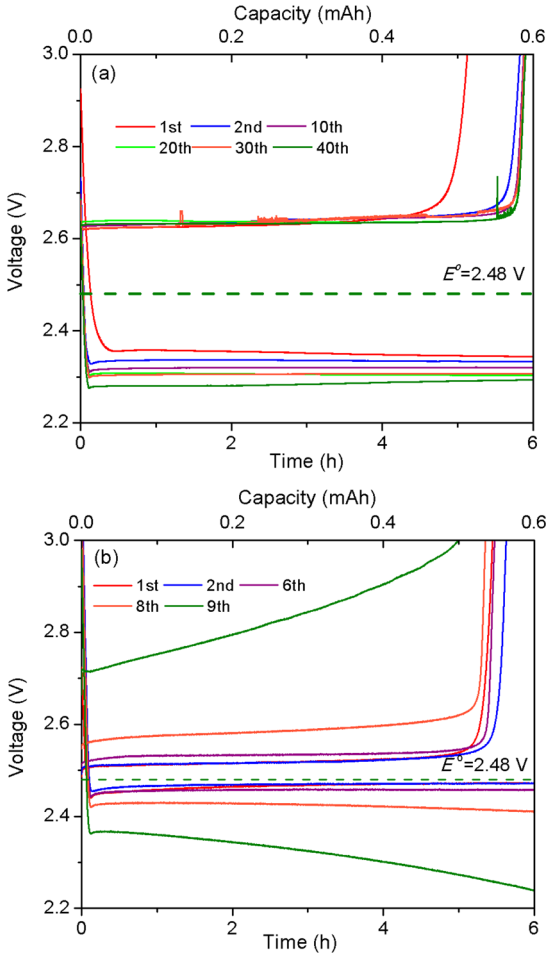

Figure 5. Voltage profiles of discharge−charge cycles of K−O_2 batteries (a) with a Nafion-K^+ membrane, (b) without a Nafion-K^+ membrane.

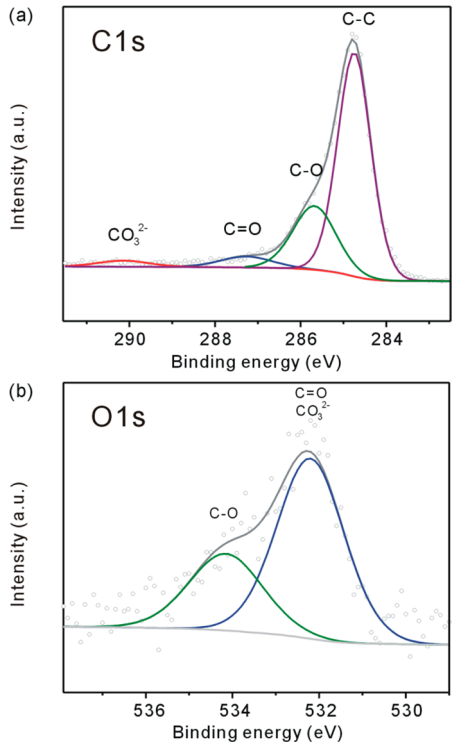

Figure 6. XPS spectra of the carbon powder in the cathode after the 48 battery cycles: (a) C 1s and (b) O 1s.

the majority of the cycles (see Figure S6 in the Supporting Information).

XPS spectra of the carbon powder utilized in the cathode (Figure 6) reveal limited growth of carbonate and carbonyl species from decomposition after 48 cycles compared to pristine carbon powder (see Figure S7 in the Supporting Information) indicating insulating species on the cathode were not formed. This supports that the decay in discharge potentials observed upon cycling is likely due to the formation of unwanted anode surface layers suppressing K^+ ion transport. The growth of the anode surface layer may also explain the voltage spikes observed upon charging, especially in later cycles. More importantly, the lower level of electrolyte and carbon cathode decompositions, as indicated by this cathode XPS result, shows the advantage of K−O_2 batteries compared to Li−O_2 batteries. In a recent study about Na−O_2 batteries based on NaO_2, it was also shown that a clearly "cleaner" cathode chemistry was observed in Na−O_2 batteries than Li−O_2 batteries.[30] Instead of forming reactive LiO_2 intermediates, the formation of stable KO_2 compound in K−O_2 batteries could reduce the decomposition of the electrolyte and carbon cathode during the discharge process. Meanwhile, the low overpotential needed for the charging process could prevent the parasitic reactions induced by high positive polarizations, as found in Li−O_2 batteries.[7]

A detailed mechanism for the cycling improvement observed with the inclusion of the polymeric membrane is complicated and will be discussed in a separate report upon further investigation. However, possible explanations include reduced oxygen crossover to the anode and restricted diffusion of anode side products to the cathode as evidenced from the improved Coulombic efficiencies (see Figure S6 in the Supporting Information). However, K^+ ion conduction in Nafion-K^+ membranes, which is likely similar to the proton conduction in a protonated Nafion membrane, still requires the aid of solvent molecules. Thus, the diffusion of nonpolar oxygen molecules is restricted, but not fully eliminated, by the nanoporous structure within the Nafion-K^+ membrane. Because O_2 crossover was not fully eliminated, a yellow anode surface layer was still observed after battery cycling. Long-term exposure of the anode to O_2 molecules remains a significant problem. Further development of K^+ ion selective materials (i.e., ceramic electrolytes) preventing oxygen crossover will hopefully solve the problem and result in significantly improved battery cycle life.

CONCLUSIONS

The surface layer growth on the potassium anode in K−O_2 batteries is proposed to be the main factor limiting battery life. By means of ATR-IR, Raman, ^{1}H NMR, ^{13}C NMR, ^{19}F-NMR, UV−vis, and volumetric titration, a detailed compositional analysis of the surface layer after aging potassium in a DME electrolyte and after battery operation was performed. The results show that the surface layer compositions were similar whether the anode was aged or cycled under battery conditions. This implies that the growth of the surface layer is due to the spontaneous interaction between the potassium metal anode, the ether solvent (DME), and O_2 molecules. Based on the side products detected in the surface layer and theoretical DFT

calculations, an electrolyte decomposition mechanism on the anode was postulated. The highly exothermic process of electron transfer from a negatively charged DME radical to an O_2 molecule that has crossed over to the anode could induce the cleavage of the C−O bonds in DME. The products generated may further react with superoxide ions or oxygen molecules to form the detected species in the anode surface layer. Introduction of a polymeric cation selective membrane, Nafion-K^+, was found to improve battery cycle life by restricting the crossover of O_2 molecules to the anode and DME radicals to the cathode. However, O_2 crossover was not completely eliminated and improved ion separation membranes must be developed to further enhance long-term operation of K−O_2 batteries.

■ ASSOCIATED CONTENT

Supporting Information

SEM, ^{39}K-NMR, EPR, additional ^{1}H NMR and XPS analysis. This material is available free of charge via the Internet at http://pubs.acs.org.

■ AUTHOR INFORMATION

Corresponding Author

*E-mail: wu@chemistry.ohio-state.edu.

Notes

The authors declare no competing financial interest.

■ ACKNOWLEDGMENTS

We are thankful for the financial support from Honda Research Institute USA. We acknowledge grants of computer time through the CNM Carbon Cluster at Argonne National Laboratory, the ALCF Fusion Cluster at Argonne National Laboratory. K.C.L. and L.A.C. were supported as part of the Joint Center for Energy Storage Research (JCESR), an Energy Innovation Hub funded by the U.S. Department of Energy, Office of Science, Basic Energy Sciences.

■ REFERENCES

(1) Abraham, K. M.; Jiang, Z. A Polymer Electrolyte-Based Rechargeable lithium/Oxygen Battery. *J. Electrochem. Soc.* **1996**, *143*, 1−5.

(2) Ogasawara, T.; Débart, A.; Holzapfel, M.; Novák, P.; Bruce, P. G. Rechargeable Li_2O_2 Electrode for Lithium Batteries. *J. Am. Chem. Soc.* **2006**, *128*, 1390−1393.

(3) Girishkumar, G.; McCloskey, B.; Luntz, A. C.; Swanson, S.; Wilcke, W. Lithium−Air Battery: Promise and Challenges. *J. Phys. Chem. Lett.* **2010**, *1*, 2193−2203.

(4) Bruce, P.; Freunberger, S. Li-O_2 and Li-S Batteries with High Energy Storage. *Nat. Mater.* **2011**, *11*, 19−29.

(5) Shao, Y.; Ding, F.; Xiao, J.; Zhang, J. J. G.; Xu, W.; Park, S.; Wang, Y.; Liu, J. Making Li-Air Batteries Rechargeable: Material Challenges. *Adv. Funct. Mater.* **2013**, *23*, 987−1004.

(6) Xu, W.; Hu, J.; Engelhard, M. H.; Towne, S. A.; Hardy, J. S.; Xiao, J.; Feng, J.; Hu, M. Y.; Zhang, J. J.-G.; Ding, F.; et al. The Stability of Organic Solvents and Carbon Electrode in Nonaqueous Li-O_2 Batteries. *J. Power Sources* **2012**, *215*, 240−247.

(7) Ottakam Thotiyl, M. M.; Freunberger, S. A.; Peng, Z.; Bruce, P. G. The Carbon Electrode in Non-Aqueous Li-O_2 Cells. *J. Am. Chem. Soc.* **2013**, *135*, 494−500.

(8) McCloskey, B.; Scheffler, R. On the Mechanism of Non-Aqueous Li-O_2 Electrochemistry on C and Its Kinetic Overpotentials: Some Implications for Li-Air Batteries. *J. Phys. Chem. C* **2012**, *116*, 23897−23905.

(9) Ren, X.; Wu, Y. A Low-Overpotential Potassium-Oxygen Battery Based on Potassium Superoxide. *J. Am. Chem. Soc.* **2013**, *135*, 2923−2926.

(10) Hartmann, P.; Bender, C. L.; Vračar, M.; Dürr, A. K.; Garsuch, A.; Janek, J.; Adelhelm, P. A Rechargeable Room-Temperature Sodium Superoxide (NaO_2) Battery. *Nat. Mater.* **2013**, *12*, 228−232.

(11) Khan, A. U.; Mahanti, S. D. Collective Electron Effects of O_2^- in Potassium Superoxide. *J. Chem. Phys.* **1975**, *63*, 2271.

(12) Viswanathan, V.; Thygesen, K. S.; Hummelshøj, J. S.; Nørskov, J. K.; Girishkumar, G.; McCloskey, B. D.; Luntz, A. C. Electrical Conductivity in Li_2O_2 and Its Role in Determining Capacity Limitations in Non-Aqueous Li-O_2 Batteries. *J. Chem. Phys.* **2011**, *135*, 214704.

(13) Luntz, A.; Viswanathan, V. Tunneling and Polaron Charge Transport through Li_2O_2 in Li−O_2 Batteries. *J. Phys. Chem. Lett.* **2013**, *4*, 3494−3499.

(14) Laoire, C. O.; Mukerjee, S.; Abraham, K. M.; Plichta, E. J.; Hendrickson, M. A. Influence of Nonaqueous Solvents on the Electrochemistry of Oxygen in the Rechargeable Lithium-Air Battery. *J. Phys. Chem. C* **2010**, *114*, 9178−9186.

(15) Hartmann, P.; Bender, C. L.; Sann, J.; Dürr, A. K.; Jansen, M.; Janek, J.; Adelhelm, P. A Comprehensive Study on the Cell Chemistry of the Sodium Superoxide (NaO_2) Battery. *Phys. Chem. Chem. Phys.* **2013**, *15*, 11661−11672.

(16) Bender, C. L.; Hartmann, P.; Vračar, M.; Adelhelm, P.; Janek, J. On the Thermodynamics, the Role of the Carbon Cathode, and the Cycle Life of the Sodium Superoxide (NaO_2) Battery. *Adv. Energy Mater.* **2014**, DOI: 10.1002/aenm.201301863.

(17) Choi, N.S. N.; Chen, Z.; Freunberger, S. A.; Ji, X.; Sun, Y. K.; Amine, K.; Yushin, G.; Nazar, L. F.; Cho, J.; Bruce, P. G. Challenges Facing Lithium Batteries and Electrical Double-Layer Capacitors. *Angew. Chem., Int. Ed.* **2012**, *51*, 9994−10024.

(18) Dainton, F.; Wiles, D.; Wright, A. Blue "solutions" of Potassium in Ethers. *J. Chem. Soc.* **1960**, 4283−4289.

(19) Grobelny, Z.; Stolarzewicz, A.; Szczepanski, M.; Sokol, M. Formation and Decomposition of Potassium Potassides Complexed Crown Ethers in Tetrahydrofuran Solution. *Curr. Org. Chem.* **2008**, *12*, 1040−1049.

(20) Shui, J. L.; Okasinski, J. S.; Kenesei, P.; Dobbs, H. A.; Zhao, D.; Almer, J. D.; Liu, D. J. Reversibility of Anodic Lithium in Rechargeable Lithium-Oxygen Batteries. *Nat. Commun.* **2013**, *4*, 2255.

(21) Assary, R. S.; Lu, J.; Du, P.; Luo, X.; Zhang, X.; Ren, Y.; Curtiss, L. A.; Amine, K. The Effect of Oxygen Crossover on the Anode of a Li-O_2 Battery Using an Ether-Based Solvent: Insights from Experimental and Computational Studies. *ChemSusChem* **2013**, *6*, 51−55.

(22) Perusich, S. FTIR Equivalent Weight Determination of Perfluorosulfonate Polymers. *J. Appl. Polym. Sci.* **2011**, *120*, 165−183.

(23) Frisch, M. J.; Trucks, G. W.; Schlegel, H. B.; Scuseria, G. E.; Robb, M. A.; Cheeseman, J. R.; Scalmani, G.; Barone, V.; Mennucci, B.; Petersson, G. A.; Nakatsuji, H.; Caricato, M.; Li, X.; Hratchian, H. P.; Izmaylov, A. F.; Bloino, J.; Zheng, G.; Sonnenberg, J. L.; Hada, M.; Ehara, M.; Toyota, K.; Fukuda, R.; Hasegawa, J.; Ishida, M.; Nakajima, T.; Honda, Y.; Kitao, O.; Nakai, H.; Vreven, T.; Montgomery, J. A., Jr.; Peralta, J. E.; Ogliaro, F.; Bearpark, M.; Heyd, J. J.; Brothers, E.; Kudin, K. N.; Staroverov, V. N.; Kobayashi, R.; Normand, J.; Raghavachari, K.; Rendell, A.; Burant, J. C.; Iyengar, S. S.; Tomasi, J.; Cossi, M.; Rega, N.; Millam, J. M.; Klene, M.; Knox, J. E.; Cross, J. B.; Bakken, V.; Adamo, C.; Jaramillo, J.; Gomperts, R.; Stratmann, R. E.; Yazyev, O.; Austin, A. J.; Cammi, R.; Pomelli, C.; Ochterski, J. W.; Martin, R. L.; Morokuma, K.; Zakrzewski, V. G.; Voth, G. A.; Salvador, P.; Dannenberg, J. J.; Dapprich, S.; Daniels, A. D.; Farkas, O.; Foresman, J. B.; Ortiz, J. V.; Cioslowski, J.; Fox, D. J. *Gaussian 09*, revision A.1; Gaussian, Inc.: Wallingford, CT, 2009.

(24) Cafasso, F.; Sundheim, B. R. Solutions of Alkali Metals in Polyethers. I. *J. Chem. Phys.* **1959**, *31*, 809−813.

(25) Panayotov, I. M.; Tsvetanov, Ch. B.; I. V, B.; R. S, V. Alkali Metal Solutions in Organic Solvents Obtained in the Presence of Polyethylene Oxide. *Die Makromol. Chemie* **1970**, *134*, 313−316.

(26) Stolarzewicz, A.; Grobelny, Z.; Grobelny, J. Characterization of Potassium and Sodium−potassium Alloy Solutions Containing Metal Anions and Complexed Cations by Means of NMR and ESR Techniques. *Spectrochim. Acta Part A* **2000**, *56*, 1257−1265.
(27) Grobelny, J.; Sokól, M.; Jedliński, Z. Complexation of Potassium Cations by Tetraglyme and 18-Crown-6 as Evidenced by ^{39}K NMR Spectroscopy. *Magn. Reson. Chem.* **1991**, *29*, 679−680.
(28) Schwenke, K. U.; Meini, S.; Wu, X.; Gasteiger, H. A.; Piana, M. Stability of Superoxide Radicals in Glyme Solvents for Non-Aqueous Li-O_2 Battery Electrolytes. *Phys. Chem. Chem. Phys.* **2013**, *15*, 11830−11839.
(29) Bryantsev, V. S.; Giordani, V.; Walker, W.; Blanco, M.; Zecevic, S.; Sasaki, K.; Uddin, J.; Addison, D.; Chase, G. V. Predicting Solvent Stability in Aprotic Electrolyte Li-Air Batteries: Nucleophilic Substitution by the Superoxide Anion Radical ($O_2^{\bullet-}$). *J. Phys. Chem. A* **2011**, *115*, 12399−12409.
(30) McCloskey, B. D.; Garcia, J. M.; Luntz, A. C. Chemical and Electrochemical Differences in Nonaqueous Li−O_2 and Na−O_2 Batteries. *J. Phys. Chem. Lett.* **2014**, *5*, 1230−1235.